HHS Public Access

Author manuscript

Biochemistry. Author manuscript; available in PMC 2018 June 26.

Published in final edited form as:

Biochemistry. 2017 September 26; 56(38): 5090–5098. doi:10.1021/acs.biochem.7b00576.

Transition State Analogue Inhibitors of 5′-Deoxyadenosine/5′-Methylthioadenosine Nucleosidase from *Mycobacterium tuberculosis*

Hilda A. Namanja-Magliano[†], **Gary B. Evans**[‡,§], **Rajesh K. Harijan**[†], **Peter C. Tyler**[‡], and **Vern L. Schramm**[*,†]

[†]Department of Biochemistry, Albert Einstein College of Medicine, 1300 Morris Park Avenue, Bronx, New York 10461, United States [‡]The Ferrier Research Institute, Victoria University of Wellington, Lower Hutt, Wellington 5040, New Zealand [§]The Maurice Wilkins Centre for Molecular Biodiscovery, The University of Auckland, Auckland, New Zealand

Abstract

Mycobacterium tuberculosis 5′-deoxyadenosine/ 5′-methylthioadenosine nucleosidase (Rv0091) catalyzes the *N*-riboside hydrolysis of its substrates 5′-methylthioadenosine (MTA) and 5′-deoxyadenosine (5′-dAdo). 5′-dAdo is the preferred substrate, a product of radical *S*-adenosylmethionine-dependent enzyme reactions. Rv0091 is characterized by a ribocation-like transition state, with low N-ribosidic bond order, an N7-protonated adenine leaving group, and an activated but weakly bonded water nucleophile. DADMe-Immucillins incorporating 5′-substituents of the substrates 5′-dAdo and MTA were synthesized and characterized as inhibitors of Rv0091. 5′-Deoxy-DADMe-Immucillin-A was the most potent among the 5′-dAdo transition state analogues with a dissociation constant of 640 pM. Among the 5′-thio substituents, hexylthio-DADMe-Immucillin-A was the best inhibitor at 87 pM. The specificity of Rv0091 for the Immucillin transition state analogues differs from those of other bacterial homologues because of an altered hydrophobic tunnel accepting the 5′-substituents. Inhibitors of Rv0091 had weak cell growth effects on *M. tuberculosis* or *Mycobacterium smegmatis* but were lethal toward *Helicobacter pylori*, where the 5′-methylthioadenosine nucleosidase is essential in menaquinone

[*]Corresponding Author: vern.schramm@einstein.yu.edu.

Supporting Information

The Supporting Information is available free of charge on the ACS Publications website at DOI: 10.1021/acs.bio-chem.7b00576. Homology model of Rv0091 and superimposition with HpMTAN and EcMTAN (Figure S1), comparison of primary sequences of Rv0091, HpMTAN, and EcMTAN (Figure S2), superimposition of the active sites of the complexes of HpMTAN and EcMTAN with BT-DADMe-ImmA, with Rv0091 modeled with BT-DADMe-ImmA and HT-DADMe-ImmA (Figure S3), and analysis of neighboring genes of Rv0091, HpMTAN, and EcMTAN (Figure S4) (PDF)

ORCID

Peter C. Tyler: 0000-0002-3151-6208

Vern L. Schramm: 0000-0002-8056-1929

Author Contributions

H.A.N.-M. and V.L.S. designed inhibitors. G.B.E. and P.C.T. designed and performed the chemical synthesis of compounds. H.A.N.-M. designed and performed inhibitor experiments. R.K.H. performed molecular modeling and docking. V.L.S. and H.A.N.-M. analyzed data. All authors contributed to the writing of the manuscript.

Notes

The authors declare no competing financial interest.

biosynthesis. We propose that Rv0091 plays a role in 5′-deoxyadenosine recycling but is not essential for growth in these *Mycobacteria*.

Graphical abstract

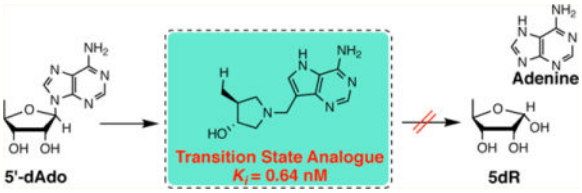

5′-Methylthioadenosine/*S*-adenosylhomocysteine nucleosi-dases (MTANs) are absent in human metabolism; however in bacteria, they are involved in pathways related to *S*-adenosylmethionine (SAM) recycling, quorum sensing, meth-ylation, and menaquinone and polyamine biosynthesis.[1–3] The MTANs catalyze *N*-ribosidic bond hydrolysis of 5′-methyl-thioadenosine (MTA), *S*-adenosylhomocysteine (SAH), and 5′-deoxyadenosine (5′-dAdo). *Mycobacterium tuberculosis* Rv0091 was originally annotated as a MTAN; however, recent studies demonstrate that it functions primarily as a 5′-dAdo nucleosidase.[4] 5′-dAdo is generated together with methionine as products of radical SAM-dependent enzyme reactions (Scheme 1).[5] The *M. tuberculosis* genome encodes 21 open reading frames annotated as radical SAM enzymes based on the sequence analysis identifying an iron–sulfur CX_3CX_2C motif that has been linked to radical SAM function.[6] Accumulation of 5′-dAdo is reported to block the activity of some SAM-related enzymes as a product inhibitor.[3]

Tuberculosis (TB) is one of the most difficult bacterial infections because of the spread of multidrug resistant strains. TB affects one-third of the world's population and is resistant to many of the current antibacterial therapies.[7] TB poses a worldwide threat, and new antibiotics are needed to treat the causative agent, *M. tuberculosis.* Here we explore the transition state analogue specificity of Rv0091 MTAN and test several inhibitors against cultured organisms as potential antibacterials.

Transition state analogues capture the geometry and electrostatic features of an enzymatic transition state in chemically stable structures. The analogues have the potential to bind to the enzyme much tighter than the substrate, with an upper limit of the factor equal to the catalytic enhancement imposed by the enzyme, relative to the Michaelis complex.[8–10] A perfect transition state analogue is impossible to design, as the actual transition state structure consists of non-equilibrium bond lengths and charge distributions that cannot be captured in a stable molecule. The Immucillins and DADMe-Immucillins are stable transition state analogues of *N*-ribosyltransferases developed via transition state analysis using kinetic isotope effects (KIEs) and computational chemistry.[11–13] Several bacterial MTANs are inhibited by these compounds with potent dissociation constants (femtomolar to picomolar range).[14–17]

Previously, the transition state structure of *M. tuberculosis* Rv0091 was analyzed and found to resemble the DADMe-Immucillins.[4] The DADMe-Immucillins contain a 5′-thio group to mimic the MTAN substrate MTA. A family of the DADMe-Immucillins inhibited Rv0091

with dissociation constants with picomolar to nanomolar affinity. 5′-dAdo was previously shown to be the preferred substrate of Rv0091; therefore, we anticipated transition state analogues similar to the transition state for 5′-dAdo to have the best affinities. In this study, we incorporate features of 5′-dAdo into transition state analogue design. Inhibition constants are established for several 5′-deoxyalkyl-DADMe-Immucillin-A compounds. Chemical synthesis and inhibition for the novel compound 5′-deoxy-DADMe-ImmA (**4**) are described. The 5′-deoxyalkyl- and 5′-thio-containing DADMe-Immucillin-A compounds (MTA and SAH substrate features) displayed dissociation constants in the picomolar to low nanomolar range. The 5′-deoxyalkyl-DADMe-Immucillin inhibitors show optimal inhibitory activity with short 5′-substituents, while 5′-thioalkyl-DADMe-Immu-cillins bind most tightly with longer 5′-substituents. This inhibitory pattern is not found in other bacterial MTANs and is therefore unique to Rv0091. Molecular modeling of inhibitors into the catalytic site of Rv0091 indicates an altered binding mode for 5′-substituents compared to those of other bacterial MTANs.

Bacterial growth assays show that Rv0091 inhibitors have weak effects on the growth of *M. tuberculosis* and *Mycobacterium smegmatis*. In contrast, the same inhibitors displayed potent antibacterial activity against *Helicobacter pylori* species. The essential nature of MTAN in menaquinone synthesis for *H. pylori* is well-documented.[17,18] Thus, the function of Rv0091 MTAN is not essential for laboratory growth in these *Mycobacteria*.

MATERIALS AND METHODS

General Experimental Approach for Inhibitor Synthesis

Compounds **5**–**20** were synthesized as previously described.[17,19–23] Air sensitive reactions were performed under argon. Organic solutions were dried over anhydrous $MgSO_4$, and the solvents were evaporated under reduced pressure. Anhydrous and chromatography solvents were obtained commercially and used without any further purification. Thin layer chromatography (TLC) was performed on glass or aluminum sheets coated with 60 F254 silica gel. Organic compounds were visualized under ultraviolet light or via the use of a dip of ammonium molybdate (5 wt %) and cerium(IV) sulfate·$4H_2O$ (0.2 wt %) in aqueous H_2SO_4 (2 M), one of I_2 (0.2%) and KI (7%) in H_2SO_4 (1 M), or one of 0.1% ninhydrin in EtOH. Chromatography (flash column) was performed on silica gel (40–63 μm) or on an automated system with a continuous gradient facility. 1H nuclear magnetic resonance (NMR) spectra were measured in $CDCl_3$, CD_3OD, DMSO-d_6 (internal Me_4Si, δ 0), or methanol-d_4 and ^{13}C NMR spectra in $CDCl_3$ (center line, δ 77.0) or CD_3OD (center line, δ 49.0). Assignments of ^1H and ^{13}C resonances were based on two-dimensional (^1H–^1H DQF-COSY, ^1H–^{13}C HSQC, or HMBC) and DEPT experiments. Positive electrospray mass spectra were recorded on a Q-TOF tandem mass spectrometer.

(3*S*,4*R*)-*tert*-Butyl-3-(bromomethyl)-4-hydroxypyrroli-dine-1-carboxylate (2) Synthesis

Methanesulfonyl chloride (0.45 mL, 5.7 mmol) was added dropwise to a stirred solution of *tert*-butyl 3-hydroxy-4-(hydroxymethyl)pyrrolidine-1-carbox-ylate (**1**) (1.13 g, 5.2 mmol) and 2,6-dimethylpyridine (1.2 mL, 10.3 mmol) in acetone (20 mL) and the mixture left to stir for 24 h. The resulting suspension was filtered to remove salt, and then lithium bromide

(2.25 g, 25.9 mmol) was added to the filtrate and the mixture refluxed for 3 h, at which time the reaction was deemed complete. The crude reaction mixture was absorbed onto silica gel (5 g) and concentrated *in vacuo* and the resulting residue purified by chromatography (20% → 40% → 100% EA/PE solvent) to afford title compound **2** (832 mg, 57%) as a syrup: ^{1}H NMR (500 MHz, $CDCl_3$) δ 4.06 (brs, 1H), 3.67 (brs, 2H), 3.47−3.36 (m, 2H), 3.28−3.18 (m, 2H), 2.50 (brs, 1H), 1.46 (s, 9H); ^{13}C NMR (125 MHz, $CDCl_3$) δ 154.6, 79.9, (73.3, 72.5), (52.6, 52.3), (48.8, 48.3), (48.2, 47.6), 32.6, 28.5; HRMS (ESI) *m*/*z* calcd for $C_{10}H_{18}NO_3BrNa^+$ 302.0368, observed 302.0364.

(3*R*,4*S*)-4-Methylpyrrolidin-3-ol (3) Synthesis

A mixture of **2**, triethylamine (1.85 mL, 13.2 mmol), and Perlman's catalyst (150 mg, 1.0 mmol) in ethanol (20 mL) was stirred under an atmosphere of hydrogen for 3 h. The crude reaction mixture was then filtered through Celite and concentrated *in vacuo* and the residue dissolved in methanol (2 mL) and concentrated HCl (2 mL) and concentrated *in vacuo*. The resulting syrup was dissolved in additional concentrated HCl (2 mL) and concentrated *in vacuo*. The residue was dissolved in MeOH, absorbed onto silica, and concentrated *in vacuo*, and the resulting solid was purified by chromatography (30% 7N NH_3 in a MeOH/$CHCl_3$ solvent) to afford title compound **3** (501 mg, 97%) as an oil: ^{1}H NMR (500 MHz, $CDCl_3$) δ 4.24 (brs, 1H), 3.65−3.55 (m, 2H), 3.25 (d, J = 15.0 Hz, 1H), 3.08−3.04 (m, 1H), 2.39 (brs, 1H), 1.09 (d, J = 10.0 Hz, 3H); ^{13}C NMR (125 MHz, $CDCl_3$) δ 75.5, 50.8, 50.2, 39.9, 15.1; HRMS (ESI) *m*/*z* calcd for $C_5H_{12}NO$ $[MH]^+$ 102.0919, observed 102.0914.

(3*R*,4*S*)-1-[(9-Deazahypoxanthin-9-yl)methyl]-3-hy-droxy-4-methylpyrrolidine (4) Synthesis

Formaldehyde (0.41 mL, 5.4 mmol, 37 mass % aqueous) was added to a stirred suspension of **3** (500 mg, 4.9 mmol) and 9-deazaadenine (77 mg 5.4 mmol) in a mixture of water (2.5 mL) and ethanol (5 mL) and then left to stir at room temperature for 48 h. The crude reaction mixture was absorbed onto silica and concentrated *in vacuo* and the solid residue purified by silica gel chromatography to afford title compound **4** (647 mg, 53%) as a solid: ^{1}H NMR (500 MHz, methanol-d_4) δ 8.18 (s, 1H), 7.49 (s, 1H), 3.87−3.74 (m, 2H), 3.37 (s, 1H), 3.05 (dd, J = 9.6, 7.7 Hz, 1H), 2.82 (dd, J = 10.4, 6.5 Hz, 1H), 2.70 (dd, J = 10.4, 4.3 Hz, 1H), 2.17 (dd, J = 9.6, 7.9 Hz, 1H), 2.04 (ht, J = 7.2, 3.5 Hz, 1H), 1.05 (d, J = 6.9 Hz, 3H); ^{13}C NMR (125 MHz, methanol-d_4) δ 152.1, 151.0, 147.0, 130.1, 115.1, 112.6, 79.0, 62.1, 61.0, 49.2, 43.0, 17.8; HRMS (ESI) *m*/*z* calcd for $C_{12}H_{18}N_4O$ $[MH]^+$ 248.1511, observed 248.1508.

Expression and Purification of 5′-Deoxyadenosine/5′-Methylthioadenosine Nucleosidase

Enzyme expression and purification were performed as described previously.[4] Briefly, *Escherichia coli* BL21 Star (DE3) plysS cell lines were employed for expression. A 25 mL initial culture in LB medium (Gibco) supplemented with ampicillin (100 μg/mL) and chloramphenicol (100 μg/mL) was incubated overnight at 37 °C. The following day, 6 mL of culture was added to 1 L of fresh LB-ampicillin (100 μg/mL) and incubated at 37 °C to an OD_{600} of 0.6–0.8. Cells were induced with 0.5 mM isopropyl D-thiogalactoside (IPTG) (Goldbio) and incubated overnight at 28 °C. Cells were harvested, and the protein was purified by Ni-NTA (Qiagen) chromatography with a 30 to 250 mM imidazole buffer

containing 20 mM Tris-HCl (pH 7.4) and 300 mM NaCl. Fractions containing purified protein (>90% as determined by a sodium dodecyl sulfate gel) were pooled, exchanged into 50 mM HEPES (pH 7.4) and 10% glycerol, and stored at −80 °C.

Dissociation Constants

Dissociation constants (K_i values) of Rv0091 inhibitors were determined as previously described.[24] Briefly, the 5′-dAdo nucleosidase reaction mixture was coupled with 1 unit of xanthine oxidase (Sigma-Aldrich) in the presence of 1 mM 5′-dAdo and varying concentrations of inhibitor in 50 mM HEPES (pH 7.4) at 25 °C. Formation of 2,8-dihydroxyadenine was monitored at 305 nm for 2 h. The reactions were initiated by adding 10 nM enzyme. The K_i values were obtained from the rates with and without inhibitors (v_i/v_o) that were fitted using the Morrison quadradic equation for tight-binding inhibitors (eq 1) in GraphPad Prism.[25] The K_M for 5′-dAdo is 10.9 μM, and [E], [I], and [S] are the enzyme, inhibitor, and substrate concentrations, respectively.[4]

$$v = v_o\left\{1 - \left[[E_T] + [I] + K_i\left(1 + \frac{[S]}{K_M}\right)\right]\right\} - \frac{\sqrt{[[E_T] + [I] + K_i\left(1 + \frac{[S]}{K_M}\right)^2 - 4[E_T][I]}}{2[E_T]} \quad (1)$$

Antibacterial Testing

M. smegmatis strain mc^{2}155 and *M. tuberculosis* strain mc^{2}6230 (nonpathogenic; pantothenate auxotroph) were cultured in Middlebrook 7H9 liquid medium (Difco) to an OD_{600} of 0.6 and plated on Middlebrook 7H10 agar plates as described previously.[26,27] Bacterial growth inhibition was assessed by a drug-diffusion method. Test compounds were added to the center of discs, placed on plates inoculated with *M. smegmatis* and *M. tuberculosis*, and allowed to grow for 96 h at 37 °C.

Antibacterial Activity Assay with *H. pylori*

H. pylori was grown under microaerophilic conditions (5% O_2, 10% CO_2, and 85% N_2) at 37 °C in brain heart infusion medium (Oxoid) with 10% fetal bovine serum (Gibco) and DENT supplement (Oxoid). HT-DADMe-ImmA and tetracycline (Sigma-Aldrich) stocks were made in culture medium, and minimum inhibitory concentration (MIC) values were determined by adding 50 μL of varied drug concentrations in a 96-well plate format at a 2× concentration in culture medium. Cultured *H. pylori* (50 μL) was added to the medium with the inhibitor. After incubation for 72 h under microaerophilic conditions at 37 °C, the OD at 600 nm was determined on a SpectraMax plate reader and MIC_{50} values were obtained using a nonlinear regression curve fit using GraphPad Prism.

Homology Modeling

An *in silico* model of Rv0091 for structure prediction was performed with I-TASSER, an online homology platform for automated protein structure prediction without any additional templates.[28] The structural comparisons of the Rv0091 model to MTAN structures that were

closely homologous were performed with the secondary structure matching (SSM) algorithm in COOT.[29] The superposition of the binding site of Rv0091 was done in comparison to *H. pylori* MTAN [HpMTAN, Protein Data Bank (PDB) entry 4FFS] and *E. coli* MTAN (EcMTAN, PDB entry 4WKC).

The Rv0091 model was analyzed by molecular docking with AutoDock Vina for binding with the transition state analogues BT-DADMe-ImmA (**13**) and HT-DADMe-ImmA (**14**).[30] Coordinates for BT-DADMe-ImmA were obtained from BT-DADMe-ImmA bound to HpMTAN (PDB entry 4FFS). Coordinates for HT-DADMe-ImmA (**14**) were generated and optimized using the eLBOW function of the PHENIX system for macromolecular structures.[31] Molecular docking was performed using a grid box of the whole protein. The potential binding site for BT-DADMe-ImmA and HT-DADMe-ImmA was identified by applying the binding mode of the inhibitors to the Rv0091 model. A second round of docking was done with the smaller grid (14 Å × 14 Å × 14 Å), centered on the binding site. The search completeness was evaluated by the default value $E = 8$ during docking with AutoDock Vina. The binding site analysis and comparisons were done with the published structures of HpMTAN (4FFS) and EcMTAN (4WKC).[17,32] The figures were made by using PyMOL (The PyMOL Molecular Graphics System, version 1.3, Schrödinger, LLC).

RESULTS AND DISCUSSION

DADMe-Immucillin Mimics of the 5′-Substituent of Rv0091 Substrates

The transition state structure of *M. tuberculosis* Rv0091 revealed a ribocation-like ribose ring with low C1′–N9 bond order, protonation of the adenine leaving group, and weak participation of the water nucleophile (Scheme 2).[4] The 5′-alkylthio-DADMe-Immucillin inhibitors resemble the Rv0091 transition state structure while incorporating features of the MTA substrate. MT-DADMe-ImmA (**11**) incorporates the 5′-methylthio group of MTA and exhibits an inhibition constant of 1.5 ± 0.4 nM (Figure 2 and Table 1). Increased hydrophobicity induced by modifying the 5′-substituent group to a 5′-hexylthio (**14**) improved the dissociation constant to 87 ± 12 pM.[4]

Enzyme catalytic theory posits that mimics of the transition state for the most proficient substrate will provide the tightest binding transition state analogue.[8] Values of k_{cat}/K_M for 5′-dAdo, MTA, and *S*-adenosylhomocysteine (SAH) with Rv0091 are reported to be 4.4×10^4, 0.6×10^4, and 0.006×10^4 M^{-1} s^{-1}, respectively. Therefore, transition state analogues of 5′-dAdo would be anticipated to have the highest affinity. The transition state structures of MTANs from *E. coli* and *Streptococcus pneumoniae* showed MTA hydrolysis to be a late dissociative process[14,15] and that of *Neisseria meningitides* to be an early S_N1 mechanism.[33] Analogues designed to mimic the early dissociative transition state are the Immucillins, characterized by a cationic N4′-imino group and a single bond between the ribocation mimic and the 9-deazapurine mimic of the leaving group. An example is MT-ImmA [**19** (Figure 2)]. The DADMe-Immucillins incorporate a methylene bridge between the ribocation mimic and the adenine leaving group analogue to more accurately mimic the transition state separation of these two groups. Their geometry resembles the fully dissociated C1′–N9 bond distance of 3.0 Å at the transition state.[13,16] The Rv0091 transition state has a C1′–N9 distance of 2.45 Å and a weakly bonded nucleophilic water, making it

intermediate between the early and late *N*-ribosyltransferase transition states.[4] The geometric preference for early or late transition state mimics was tested with the MTA transition state mimics, MT-ImmA (**19**) and MT-DADMe-ImmA (**11**). The K_i values were 85 nM for **19** and 1.5 nM for **11**, demonstrating the DADMe-Immucillin analogues more closely mimic the Rv0091 transition state, consistent with the transition state analysis.[4] Here we further explore the DADMe-ImmA analogues but extend their structural features to 5′-dAdo, the preferred substrate.

The catalytic activity of Rv0091 with 5′-dAdo as a substrate is relatively inefficient. Like many enzymes from *M. tuberculosis*, it displays a relatively low catalytic efficiency (k_{cat}/K_M) of 4.4×10^4 M^{-1} s^{-1}; however, this is 7-fold better than for MTA and 730-fold better than for SAH. 5′-Alkylthio-DADMe-Immucil-lin-A inhibitors mimic the MTA substrate at the transition state and gave K_i constants in the picomolar to low nanomolar range.[4] Transition state analogues of the 5′-dAdo substrate were obtained by the synthesis of 5′-deoxy-DADMe-ImmA (**4**) and its analogues (Scheme 3). The most similar analogue of the 5′-dAdo transition state (**4**) was a potent inhibitor with a dissociation constant of 0.64 nM (Figure 1).

Crystal structures of *Salmonella enterica*[34] and *H. pylori*[17] MTANs contain hydrophobic tunnels from the 5′-position of bound nucleosides, reaching to the solvent. This structure can accommodate a variety of hydrophobic 5′-substituents. We increased the hydrophobicity at the 5′-substituent position; as previously described, 5′-thio-DADMe-ImmA analogues (**11**–**15**) showed favorable binding properties for this change. This is also the case for the 5′-thio-DADMe-ImmA analogues with Rv0091 MTAN. For example, HT-DADMe-ImmA (**14**) bound 17 times tighter than MT-DADMe-ImmA (**11**) did (Table 1).[4] However, the hydrophobicity of the 5′-alkyl substituent did not result in improved inhibitor potency for Rv0091 (Figure 2 and Table 1). The more hydrophobic 5′-substituent compounds (**5**, **7**, and **8)** had inhibition constants slightly weaker than those of the shorter 5′-substituted **4**. Compound **9** containing the longest, but hydrophilic, substituent (PEG) was the weakest inhibitor, with a K_i of >300 nM. In comparison, **15**, which contains a 5′-thio PEG substituent, had a better potency of 8.2 ± 0.3 nM. These results suggest that the 5′-binding site of Rv0091 is unlike those of other MTANs in that it prefers 5′-alkyl substituents over 5′-thio substituents if the 5′-substituent is short. When the substituent is longer, the 5′-thio substituents are preferred.

Preference for (3*R*,4*S*) Stereochemistry in the DADMe-Immucillin Inhibitors

The stereochemistry of the 3-hydroxy-4-alkylpyrrolidine moiety with respect to inhibitor potency was explored. *trans*-Racemate compound **5** was compared to *cis*-racemate **6** and was shown to be 13-fold more potent, demonstrating that the *trans* stereochemistry is preferred at the 3-hydroxy-4-alkylpyrrolidine position. To evaluate the preference of (3*R*,4*S*) over (3*S*,4*R*) stereo-chemistry, the enantiopure (3*R*,4*S*)-MT-DADMe-ImmA (**11**) was compared to the enantiomer (3*S*,4*R*)-MT-DADMe-ImmA (**20**). **11** inhibits Rv0091 with a good potency of 1.5 nM, while compound **20** had no activity at concentrations of ≤400 μM. This observation is consistent with previous findings where (3*R*,4*S*) inhibitors displayed

potencies better than those of their enantiomeric counterparts toward other MTAN nucleosidases, including that from *E. coli*.[34]

The affinities of these transition state analogues for Rv0091 (87 pM for the best compound) and other bacterial MTANs, such as *E. coli* MTAN (femtomolar range for best compounds),[20,35] establish a reduced affinity for Rv0091. This difference can be attributed to relative catalytic efficiencies of the *E. coli* and *M. tuberculosis* enzymes. Wolfenden and Snider[9,10] postulated that the binding of transition state analogues is associated with enzyme catalytic efficiency. *E. coli* MTAN has a high catalytic efficiency of 4.7×10^7 M^{-1} s^{-1} for MTA, approximately 1000-fold more efficient than Rv0091 for 5′-dAdo.[4] The *E. coli* MTAN is also more efficient for 5′-dAdo than Rv0091 is even though it is not a preferred substrate. Consequently, transition state analogues mimicking both MTA and the 5′-dAdo substrate are known to bind more tightly for the *E. coli* enzyme by several orders of magnitude. This binding is also consistent with previous observations for the inhibitor profiles of the slow *S. pneumonia* MTAN (SpMTAN).[36]

Molecular Modeling and Putative Binding Site Residue Identification

The crystal structure of Rv0091 from *M. tuberculosis* is not available. The binding interactions of active site residues for Rv0091 were probed by docking the transition state analogue inhibitors BT-DADMe-ImmA and HT-DADMe-ImmA to explain the difference in 5′-substituent interactions from the specificity known for *H. pylori* and *E. coli* MTANs. The *in silico* model of Rv0091 was generated by the I-TESSER server (Figure S1). The best structural model of Rv0091 was obtained with a *C* score of 0.43 (the ideal *C* score is between −5 and 2; a score of 0.43 is an excellent match) and a TM score of 0.77 ± 0.10. The model has a structural fold similar to those seen in other MTANs with the exception of an extended loop (from Leu148 to Pro162) unique to Rv0091 (Figures S1 and S2). The sequence of Rv0091 is 29 and 32% identical with those of *H. pylori* and *E. coli* MTANs, respectively (Figure S2). Comparison of the Rv0091 model with *H. pylori* and *E. coli* MTANs gave root-mean-square deviations between 0.96 and 1.03 Å without and with the Rv0091 external loop, respectively.

Crystal structures of *H. pylori* and *E. coli* MTAN in complex with BT-DADMe-ImmA have been published.[24,32] Autodoc-Vina was used for the *in silico* docking of BT-DADMe-ImmA and HT-DADMe-ImmA to the binding site of Rv0091. The best fit of the interactions between the inhibitor and Rv0091 was selected from the top-ranked cluster by binding affinities. Active site superimposition of BT-DADMe-ImmA bound to HpMTAN and EcMTAN with Rv0091 modeled with both BT-DADMe-ImmA and HT-DADMe-ImmA shows the pyrrolidine and deazaadenine inhibitor groups bind in the same orientation in all the MTANs (Figure 3 and Figure S3). The catalytic site geometries of 5′-alkylthio inhibitor groups differ considerably for Rv0091. Active site tunnel residues Ile52 (in HpMTAN) and Ile50 (at the same position in EcMTAN) have nonpolar interactions with the 5′-alkylthio group of BT-DADMe-ImmA. This interaction is disrupted by the larger Met52 residue in this position in Rv0091 MTAN. The side chain of the Met52 creates a steric clash with the 5′-alkylthio group of the inhibitors to displace it relative to its geometry in EcMTAN and HpMTAN (Figure 3).

Inhibitors modeled into Rv0091 show the 3′-hydroxyl group to be hydrogen-bonded to Glu197. N1 and N3 of the 9-deazaadenine ring have hydrogen bonding interactions with the backbone nitrogen of Leu176 and Glu195, respectively. The N6 amino and N7 of the inhibitors form hydrogen bond interactions with both the peptide bond NH group of Leu176 and the side chain hydroxyl group of Asp220 (Figure 3 and Figure S3). These groups are conserved among Rv0091, HpMTAN, and EcMTAN, supporting the major divergence of Rv0091 being related to the hydrophobic region in the catalytic site that accommodates the 5′-alkylthio groups. The dissociation constant for BT-DADMe-ImmA is 1.3 nM, which is 15 times weaker binding than that of HT-DADMe-ImmA (K_d = 87 pM). HT-DADMe-ImmA has two additional carbons at the 5′-alkylthio group that make additional hydrophobic contacts with the enzyme and contribute to the higher affinity of HT-DADMe-ImmA. From the model, the butylthio group of BT-DADMe-ImmA predicts van der Waals interactions with eight amino acids, Ile11, Met52, Met196, Pro119, Tyr113, Val104, Tyr175, and Phe230. These along with two additional contacts with Glu108 and Val105 are predicted for the hexylthio group of HT-DADMe-ImmA, consistent with its tighter binding.

Antibiotic Activity against *Mycobacterium* Species and *H. pylori*

The antibacterial activity of DADMe-Immucillin compounds was investigated in a disc-diffusion assay against *M. tuberculosis* mc^{2}6230 and *M. smegmatis* mc^{2}155 strains.[37] HT-DADMe-ImmA (**14**) is the most potent inhibitor toward Rv0091 and displayed a small zone of clearance at 1000 μg/mL in both *Mycobacterium* species (Figure 4A,B). Kanamycin as an antibiotic control displayed large zones of clearance at 100 μg/ mL. Other DADMe-Immucillin compounds showed results similar to those of HT-DADMe-ImmA (**14**), indicating that the function of Rv0091 is not essential for the growth of *Mycobacteria*. This finding is in agreement with previous gene deletion experiments in *M. tuberculosis*, where Rv0091 was found to be nonessential for growth or infection.[38,39] Unlike *Mycobacteria*, MTAN has an essential function in menaquinone synthesis in *H. pylori*.[17] We tested HT-DADMe-ImmA (**14**) in a cultured cell assay using *H. pylori* with tetracycline as a control. HT-DADMe-ImmA (**14**) exhibited antibacterial activity against *H. pylori* with an IC_{50} of 13.0 ± 1.8 ng/mL (equivalent to 35 ± 5 nM), which is 6 times more potent than tetracycline as an antibiotic (Figure 4C).

Genomic Context of Rv0091

MTAN in *E. coli* has been reported to be involved in SAH and MTA recycling and in quorum sensing pathways.[2] BT-DADMe-ImmA (**13**) inhibited production of the quorum sensing signaling molecule auto-inducer (AI-2) but was not toxic to *E. coli* or *Vibrio cholerae* growth, providing support for its role in quorum sensing.[1] Comparison of the gene maps for Rv0091 (NCBI gene 886953), EcMTAN (NCBI gene 948542), and HpMTAN (NCBI gene 900251) indicates no organized operon function. In *E. coli*, the open reading frame for MTAN is adjacent to *btuF*, expressing a periplasmic B_{12} binding protein, and *dgt*, known to express a dGTP triphosphohydrolase (Figure S4). In *H. pylori*, the adjacent Hp0090 is a malonyl-CoA:acyl carrier protein transacylase. Near the Rv0091 locus in *M. tuberculosis*, a nearby open reading frame, the sequence of amino acids 32–146 (of 197) of Rv0089 is 41% identical with that of the *E. coli* BioC protein, a SAM-dependent malonyl-acyl carrier protein methyltransferase, an early step in biotin synthesis.[40] In *E. coli*, the BioC

protein is expressed from the *bioC* gene within the *bioABFCD* operon.[41] On the basis of the local gene organization near Rv0091, no insight is provided to its biological function, supporting a role in removing the 5′-dAdo product from the 21 potential radical SAM proteins in *M. tuberculosis*.

CONCLUSIONS

Transition state analogues with geometries and charges thatresemble those of the transition state for hydrolysis of 5′-dAdo by Rv0091 were synthesized and found to bind with picomolar to nanomolar dissociation constants. (*3R*,4*S*)-3-Hydroxy-4-alkylpyrrolidine stereochemistry is preferred for these compounds, consistent with findings for related bacterial MTANs.[34] Comparison of 5′-alkylthio-DADMe-ImmA inhibitors that mimic the MTA substrate provided insight into the relative specificity for 5′-dAdo and 5′-methylthio adenosine substituents for Rv0091. Short chain 5′-substituents are preferred for the 5′-deoxyalkyl inhibitors, while longer hydrophobic chains displayed tighter binding for the 5′-alkylthio inhibitors. In both cases, substitution of polar atoms into the 5′-substituent, i.e., CH_2 to O, reduces the potency of the inhibitors. *In silico* docking of BT-DADMe-ImmA (13) and HT-DADMe-ImmA (14) with a model of Rv0091 showed similar binding to *E. coli* and *H. pylori* MTAN of the pyrrolidine and deazaadenine moieties, but they differed at the 5′-alkyl or 5′-alkylthio groups. This difference is due to a methionine steric clash near the 5′- substituent in the catalytic site of Rv0091. Isoleucine is present at this position in the MTANs from *E. coli* or H. pylori. Furthermore, the weak antibacterial activity of these inhibitors against *Mycobacteria* indicates that Rv0091 functions in a nonessential pathway for growth.

Supplementary Material

Refer to Web version on PubMed Central for supplementary material.

Acknowledgments

We acknowledge Drs. Scott Cameron (Albert Einstein College of Medicine) for valuable discussions and A. Malek (Albert Einstein College of Medicine) for help with the disc-diffusion assays. *M. smegmatis* mc^2155 and *M. tuberculosis* $mc^2$6230 strains were gifts from the laboratory of Dr. William Jacobs (Albert Einstein College of Medicine).

Funding

This work was supported by National Institutes of Health Grant GM041916 and by the Michael Price Family Foundation.

ABBREVIATIONS

MTANs	5′-methylthioadenosine/*S*-adenosylhomocysteine nucleosidases
MTA	5′-methylthioadenosine
SAH	*S*-adenosyl-homocysteine
5′-dAdo	5′-deoxyadenosine

PEG	polyethylene glycol
SAM	*S*-adenosylmethionine
KIE	kinetic isotope effect

References

1. Gutierrez JA, Crowder T, Rinaldo-Matthis A, Ho MC, Almo SC, Schramm VL. Transition state analogs of 5′-methylthioadenosine nucleosidase disrupt quorum sensing. Nat Chem Biol. 2009; 5:251–257. [PubMed: 19270684]
2. Parveen N, Cornell KA. Methylthioadenosine/S-adenosylhomocysteine nucleosidase, a critical enzyme for bacterial metabolism. Mol Microbiol. 2011; 79:7–20. [PubMed: 21166890]
3. Choi-Rhee E, Cronan JE. A nucleosidase required for in vivo function of the S-adenosyl-L-methionine radical enzyme, biotin synthase. Chem Biol. 2005; 12:589–593. [PubMed: 15911379]
4. Namanja-Magliano HA, Stratton CF, Schramm VL. Transition state structure and inhibition of Rv0091, a 5′-deoxyadenosine/5′-methylthioadenosine nucleosidase from *Mycobacterium tuberculosis*. ACS Chem Biol. 2016; 11:1669–1676. [PubMed: 27019223]
5. Wang J, Woldring RP, Roman-Melendez GD, McClain AM, Alzua BR, Marsh EN. Recent advances in radical SAM enzymology: new structures and mechanisms. ACS Chem Biol. 2014; 9:1929–1938. [PubMed: 25009947]
6. Akiva E, Brown S, Almonacid DE, Barber AE 2nd, Custer AF, Hicks MA, Huang CC, Lauck F, Mashiyama ST, Meng EC, Mischel D, Morris JH, Ojha S, Schnoes AM, Stryke D, Yunes JM, Ferrin TE, Holliday GL, Babbitt PC. The structure-function linkage database. Nucleic Acids Res. 2014; 42:D521–530. [PubMed: 24271399]
7. McBryde ES, Meehan MT, Doan TN, Ragonnet R, Marais BJ, Guernier V, Trauer JM. The risk of global epidemic replacement with drug-resistant Mycobacterium tuberculosis strains. Int J Infect Dis. 2017; 56:14–20. [PubMed: 28163165]
8. Wolfenden R. Transition state analog inhibitors and enzyme catalysis. Annu Rev Biophys Bioeng. 1976; 5:271–306. [PubMed: 7991]
9. Wolfenden R. Transition state analogues for enzyme catalysis. Nature. 1969; 223:704–705. [PubMed: 4979456]
10. Wolfenden R, Snider MJ. The depth of chemical time and the power of enzymes as catalysts. Acc Chem Res. 2001; 34:938–945. [PubMed: 11747411]
11. Schramm VL. Enzymatic transition state theory and transition state analogue design. J Biol Chem. 2007; 282:28297–28300. [PubMed: 17690091]
12. Schramm VL. Enzymatic transition states and transition state analog design. Annu Rev Biochem. 1998; 67:693–720. [PubMed: 9759501]
13. Schramm VL. Enzymatic transition-state analysis and transition-state analogs. Methods Enzymol. 1999; 308:301–355. [PubMed: 10507010]
14. Singh V, Lee JE, Nunez S, Howell PL, Schramm VL. Transition state structure of 5′-methylthioadenosine/S-adenosylhomocysteine nucleosidase from *Escherichia coli* and its similarity to transition state analogues. Biochemistry. 2005; 44:11647–11659. [PubMed: 16128565]
15. Singh V, Schramm VL. Transition-state analysis of *S. pneumoniae* 5′-methylthioadenosine nucleosidase. J Am Chem Soc. 2007; 129:2783–2795. [PubMed: 17298059]
16. Gutierrez JA, Luo M, Singh V, Li L, Brown RL, Norris GE, Evans GB, Furneaux RH, Tyler PC, Painter GF, Lenz DH, Schramm VL. Picomolar inhibitors as transition-state probes of 5′-methylthioadenosine nucleosidases. ACS Chem Biol. 2007; 2:725–734. [PubMed: 18030989]
17. Wang S, Cameron SA, Clinch K, Evans GB, Wu Z, Schramm VL, Tyler PC. New Antibiotic Candidates against *Helicobacter pylori*. J Am Chem Soc. 2015; 137:14275–14280. [PubMed: 26494017]

18. Dairi T. An alternative menaquinone biosynthetic pathway operating in microorganisms: an attractive target for drug discovery to pathogenic *Helicobacter* and *Chlamydia* strains. J Antibiot. 2009; 62:347–352. [PubMed: 19557031]
19. Longshaw AI, Adanitsch F, Gutierrez JA, Evans GB, Tyler PC, Schramm VI. Design and synthesis of potent ″sulfur-free″ transition state analogue inhibitors of 5′-methylthioade-nosine nucleosidase and 5′-methylthioadenosine phosphorylase. J Med Chem. 2010; 53:6730–6746. [PubMed: 20718423]
20. Singh V, Evans GB, Lenz DH, Mason JM, Clinch K, Mee S, Painter GF, Tyler PC, Furneaux RH, Lee JE, Howell PL, Schramm VL. Femtomolar transition state analogue inhibitors of 5′-methylthioadenosine/S-adenosylhomocys-teine nucleosidase from *Escherichia coli*. J Biol Chem. 2005; 280:18265–18273. [PubMed: 15749708]
21. Haapalainen AM, Thomas K, Tyler PC, Evans GB, Almo SC, Schramm VL. *Salmonella enterica* MTAN at 1.36 angstrom resolution: a structure-based design of tailored transition state analogs. Structure. 2013; 21:963–974. [PubMed: 23685211]
22. Singh V, Evans GB, Furneaux RH, Tyler PC, Schramm VL. Targeting polyamine biosynthesis: Transition state of 5′-deoxy-5′-methylthioadenosine phosphorylase (MTAP) and transition state analogue inhibitors. Biochemistry. 2003; 42:8625.
23. Evans GB, Cameron SA, Luxenburger A, Guan R, Suarez J, Thomas K, Schramm VL, Tyler PC. Tight binding enantiomers of pre-clinical drug candidates. Bioorg Med Chem. 2015; 23:5326–5333. [PubMed: 26260335]
24. Thomas K, Cameron SA, Almo SC, Burgos ES, Gulab SA, Schramm VL. Active site and remote contributions to catalysis in methylthioadenosine nucleosidases. Biochemistry. 2015; 54:2520–2529. [PubMed: 25806409]
25. Morrison JF, Walsh CT. The behavior and significance of slow-binding enzyme inhibitors. Adv Enzymol Relat Areas Mol Biol. 2006; 61:201–301.
26. Larsen, MH., Biermann, K., Jacobs, WR, Jr. Current Protocols in Microbiology. Wiley; New York: 2007. Laboratory maintenance of *Mycobacterium tuberculosis*; p. 11Chapter 10, Unit 10A
27. Sambandamurthy VK, Wang X, Chen B, Russell RG, Derrick S, Collins FM, Morris SL, Jacobs WR Jr. A pantothenate auxotroph of *Mycobacterium tuberculosis* is highly attenuated and protects mice against tuberculosis. Nat Med. 2002; 8:1171–1174. [PubMed: 12219086]
28. Roy A, Kucukural A, Zhang Y. I-TASSER: a unified platform for automated protein structure and function prediction. Nat Protoc. 2010; 5:725–738. [PubMed: 20360767]
29. Emsley P, Cowtan K. Coot: model-building tools for molecular graphics. Acta Crystallogr, Sect D: Biol Crystallogr. 2004; 60:2126–2132. [PubMed: 15572765]
30. Trott O, Olson AJ. AutoDock Vina: improving the speed and accuracy of docking with a new scoring function, efficient optimization, and multithreading. J Comput Chem. 2010; 31:455–461. [PubMed: 19499576]
31. Adams PD, Afonine PV, Bunkoczi G, Chen VB, Davis IW, Echols N, Headd JJ, Hung LW, Kapral GJ, Grosse-Kunstleve RW, McCoy AJ, Moriarty NW, Oeffner R, Read RJ, Richardson DC, Richardson JS, Terwilliger TC, Zwart PH. PHENIX: a comprehensive Python-based system for macromolecular structure solution. Acta Crystallogr, Sect D: Biol Crystallogr. 2010; 66:213–221. [PubMed: 20124702]
32. Wang S, Haapalainen AM, Yan F, Du Q, Tyler PC, Evans GB, Rinaldo-Matthis A, Brown RL, Norris GE, Almo SC, Schramm VL. A picomolar transition state analogue inhibitor of MTAN as a specific antibiotic for *Helicobacter pylori*. Biochemistry. 2012; 51:6892–6894. [PubMed: 22891633]
33. Singh V, Luo M, Brown RL, Norris GE, Schramm VL. Transition-state structure of *Neisseria meningitides* 5′-methylthioadenosine/S-adenosylhomocysteine nucleosidase. J Am Chem Soc. 2007; 129:13831–13833. [PubMed: 17956098]
34. Evans GB, Cameron SA, Luxenburger A, Guan R, Suarez J, Thomas K, Schramm VL, Tyler PC. Tight binding enantiomers of pre-clinical drug candidates. Bioorg Med Chem. 2015; 23:5326–5333. [PubMed: 26260335]
35. Lee JE, Singh V, Evans GB, Tyler PC, Furneaux RH, Cornell KA, Riscoe MK, Schramm VL, Howell PL. Structural rationale for the affinity of pico- and femtomolar transition state analogues

of *Escherichia coli* 5′-methylthioadenosine/S-adenosylhomocysteine nucleosidase. J Biol Chem. 2005; 280:18274–18282. [PubMed: 15746096]

36. Singh V, Shi W, Almo SC, Evans GB, Furneaux RH, Tyler PC, Painter GF, Lenz DH, Mee S, Zheng R, Schramm VL. Structure and inhibition of a quorum sensing target from *Streptococcus pneumoniae*. Biochemistry. 2006; 45:12929–12941. [PubMed: 17059210]
37. Shiloh MU, DiGiuseppe Champion PA. To catch a killer. What can mycobacterial models teach us about *Mycobacterium tuberculosis* pathogenesis? Curr Opin Microbiol. 2010; 13:86–92. [PubMed: 20036184]
38. Sassetti CM, Rubin EJ. Genetic requirements for mycobacterial survival during infection. Proc Natl Acad Sci U S A. 2003; 100:12989–12994. [PubMed: 14569030]
39. Griffin JE, Gawronski JD, Dejesus MA, Ioerger TR, Akerley BJ, Sassetti CM. High-resolution phenotypic profiling defines genes essential for mycobacterial growth and cholesterol catabolism. PLoS Pathog. 2011; 7(9):e1002251. [PubMed: 21980284]
40. Lin S, Cronan JE. The BioC O-methyltransferase catalyzes methyl esterification of malonyl-acyl carrier protein, an essential step in biotin synthesis. J Biol Chem. 2012; 287:37010–37020. [PubMed: 22965231]
41. Cao X, Zhu L, Hu Z, Cronan JE. Expression and activity of the BioH esterase of biotin synthesis is independent of genome context. Sci Rep. 2017; 7:2141. [PubMed: 28526858]

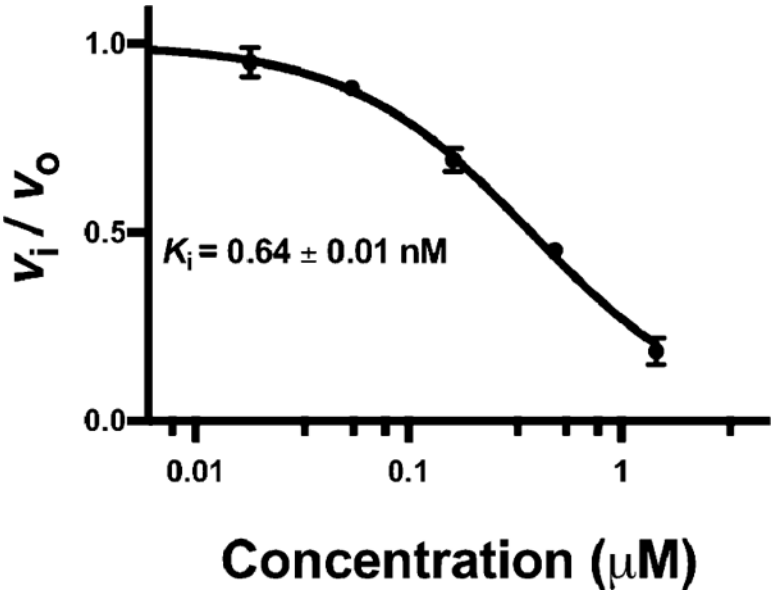

Figure 1.

Inhibition of Rv0091 by 5′-deoxy-DADMe-Immucillin-A (**4**). The reaction rate and inhibition were monitored at 305 nm for the conversion of 5′-dAdo to 2,8-dihydroxyadenine in a reaction coupled to xanthine oxidase as described in Materials and Methods. The K_i value was calculated from the fit to the Morrison equation for tight-binding inhibitors.[25] The excess substrate (1.0 mM) relative to its K_m value of 10.9 μM alters the apparent K_i by a factor of 93 for this competitive inhibitor. The true K_i of 0.64 nM is shown.

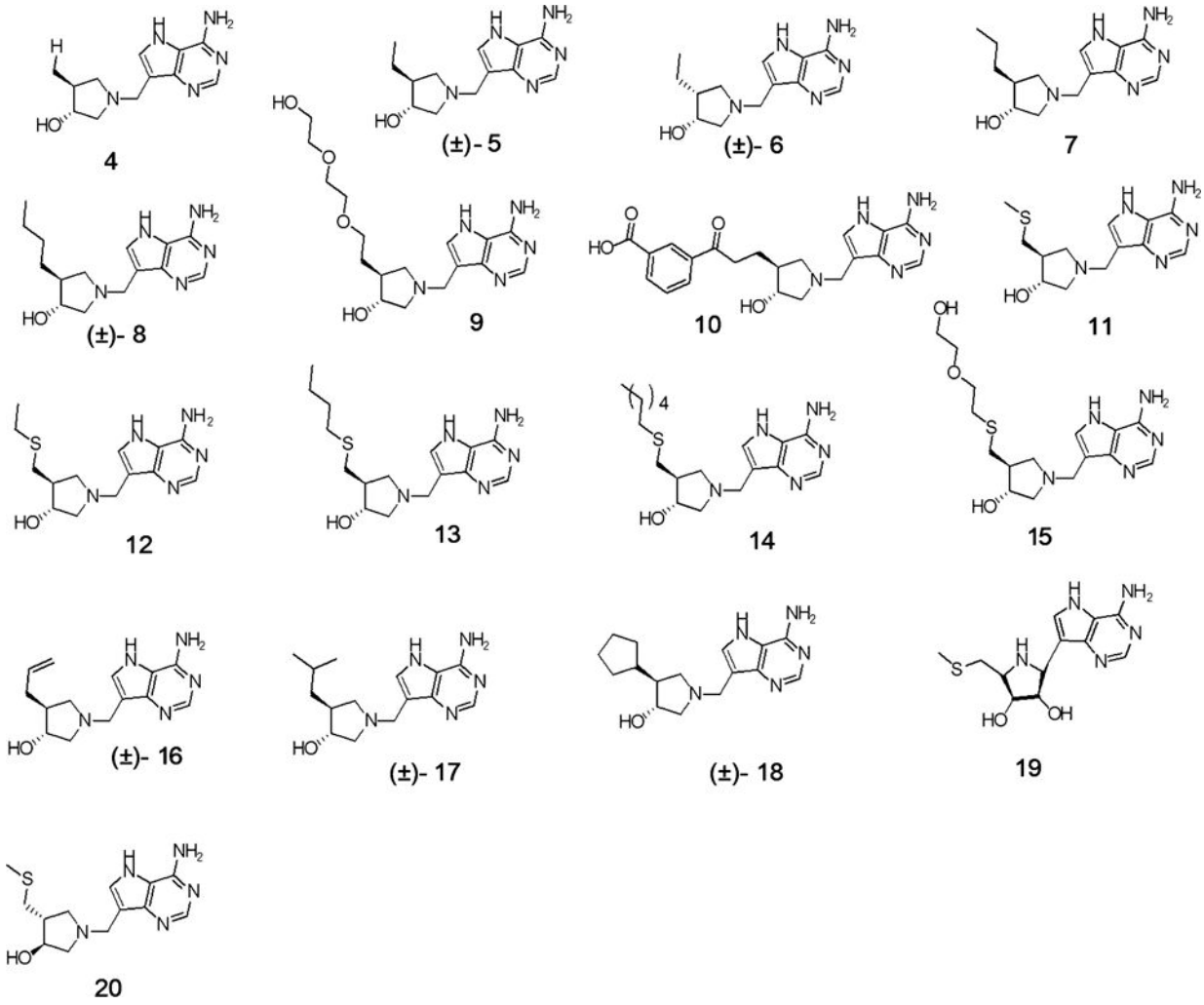

Figure 2.

DADMe-Immucillin and Immucillin-based inhibitors of Rv0091. **4**, **7**, **9**–**15**, **19**, and **20** are enantiopure compounds, and **5**, **6**, **8**, and **16**–**18** are racemic mixtures of 3-hydroxy-4-alkylpyrrolidine. Abbreviated names for some of these compounds are provided in the text.

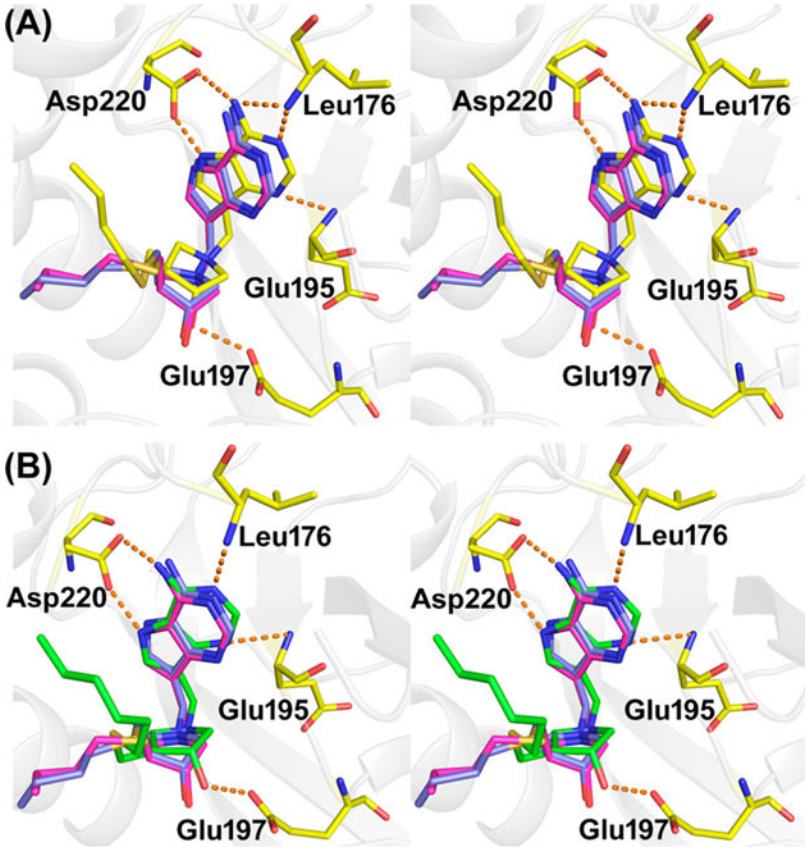

Figure 3.

Stereoview superimposition of the active sites of *H. pylori* and *E. coli* MTAN in complex with BT-DADMe-ImmA compared with Rv0091. The interactions of binding site residues of Rv0091 modeled with BT-DADMe-ImmA (yellow, panel A) and with HT-DADMe-ImmA (green, panel B) are highlighted. The BT-DADMe-ImmA compounds of *H. pylori* and *E. coli* are colored blue and pink, respectively.

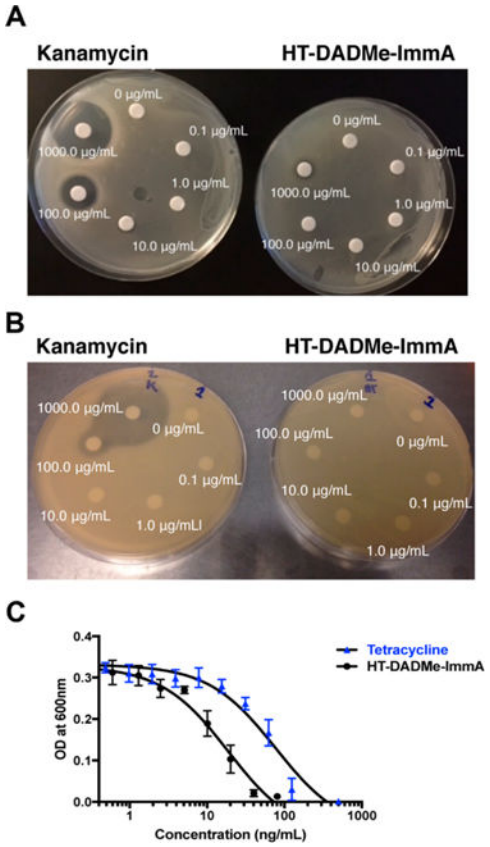

Figure 4.

Antibacterial activity. Transition state analogue HT-DADMe-ImmA (**14**) and an antibiotic control were tested for growth inhibition against (A) *M. smegmatis* mc^2155 and (B) *M. tuberculosis* mc^26230 in a disc-diffusion assay by growth for 96 h at 37 °C on agar plates. (C) Inhibition of *H. pylori* (J99) growth at 37 °C in a liquid culture by HT-DADMe-ImmA (**14**) and tetracycline. Growth was evaluated at OD = 600 nm, and MIC_{50} values were calculated by nonlinear regression using GraphPad Prism 7.

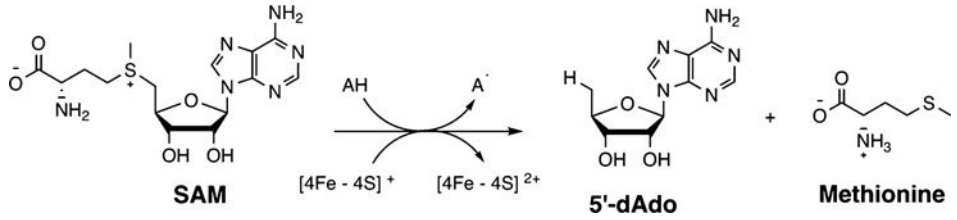

Scheme 1.

Reaction Catalyzed by Radical SAM Enzymes for the Reductive Cleavage of SAM with $[4Fe\text{-}4S]^{+}$ in the Presence of Substrate [AH] To Give 5′-dAdo and Methionine

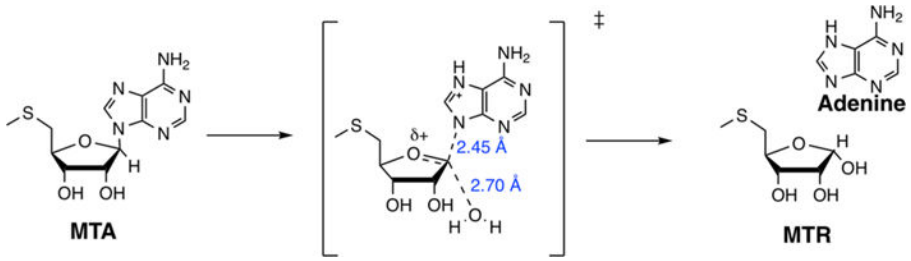

Scheme 2. Reaction and Transition State Catalyzed by Rv0091 To Give Adenine and 5-Methylthioribose (MTR)[a]

[a]The reaction goes through a transition state characterized by a ribocation character, protonation of the adenine leaving group, weak but significant participation of the nucleophilic water, and advanced loss of the C1′–N9 bond.[4]

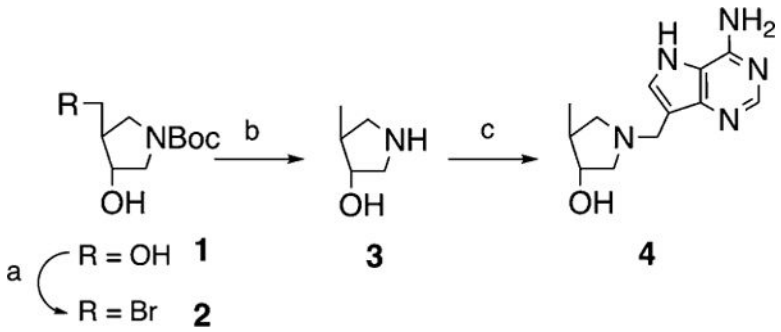

Scheme 3. Synthesis of 5′-Deoxy-DADMe-Immucillin-A (4)[a]

[a]Reagents: (a) (i) MsCl, 2,6-dimethylpyridine, acetone, room temperature; (ii) NaBr, 57% for two steps; (b) (i) $Pd(OH)_2$, H_2 (g), EtOH, room temperature; (ii) cHCl, room temperature, 97% yield for two steps; (c) 9-deazaadenine, 37% aqueous formaldehyde, H_2O, EtOH, room temperature, 53% yield.

Table 1

Inhibition of Rv0091 with DADMe-Immucillin Analogues

compound	K_i (nM)[a]	compound	K_i (nM)[a]
4	0.64 ± 0.01	**13**	1.3 ± 0.1[4]
5	1.5 ± 0.1	**14**	0.087 ± 0.012[4]
6	18.9 ± 1.1	**15**	8.2 ± 0.3
7	0.74 ± 0.05	**16**	6.7 ± 0.3
8	1.64 ± 0.20	**17**	2.8 ± 0.2
9	>300	**18**	13.5 ± 1.2
10	5.0 ± 1.1	**19**	85 ± 11[4]
11	1.5 ± 0.4[4]	**20**	NI[b]
12	13.9 ± 2.4		

[a]Dissociation constants are obtained from the xanthine oxidase coupled assay at 25 °C. The K_i value was calculated by using eq 1 for analysis of tight-binding inhibitors.[25]

[b]Not inhibited up to 400 μM.